Supporting Information for "Interseismic Strain Accumulation across the Main Recent Fault, SW Iran, from Sentinel-1 InSAR Observations"

Andrew R. Watson[1], John R. Elliott[1], Richard J. Walters[2]

[1]COMET, School of Earth and Environment, University of Leeds, UK

[2]COMET, Department of Earth Sciences, Durham University, UK

Contents of this file

1. Introduction
2. Figures S1 to S12
3. Table S1

Introduction

This supporting information provides additional figures as referenced in the main article.

Figures S2–6 show the velocities and various noise indices generated by LiCSBAS for each frame. From left to right, the top row of each shows the masked velocities (*vel.mskd*), unmasked velocities (*vel*), the mask (*mask*), and the average coherence (*coh_avg*). The middle row shows the number of used unwrapped pixels (*n_unw*), the bootstrapped standard deviation (*vstd*), the maximum network length (*maxTlen*), and the number of network gaps (*n_gap*). The bottom row shows the spatio-temporal consistency (*stc*), the number of interferograms with no loops (*n_ifg_noloop*), the number of unclosed loops (*n_loop_err*), and the root-mean-square of the residuals (*resid_rms*). Further details can be found in Table 1 of Morishita et al. (2020).

Thresholds on each of the noise indices are used to produce a mask for the velocities. We use the default values for each with the exception of *n_loop_err*, which we increase from 5 to 20, reducing the number of pixels covered by the mask. *n_loop_err* is the number of unclosed loops (those with a root-mean-square loop phase above 1.5 radians) after the loop closure check in Step 1-2 of LiCSBAS, which primarily relates to unwrapping errors. We consider the increase of this threshold acceptable considering the large number of interferograms (650–1000) and resulting loops (approximately 2000 for 006D) within our networks.

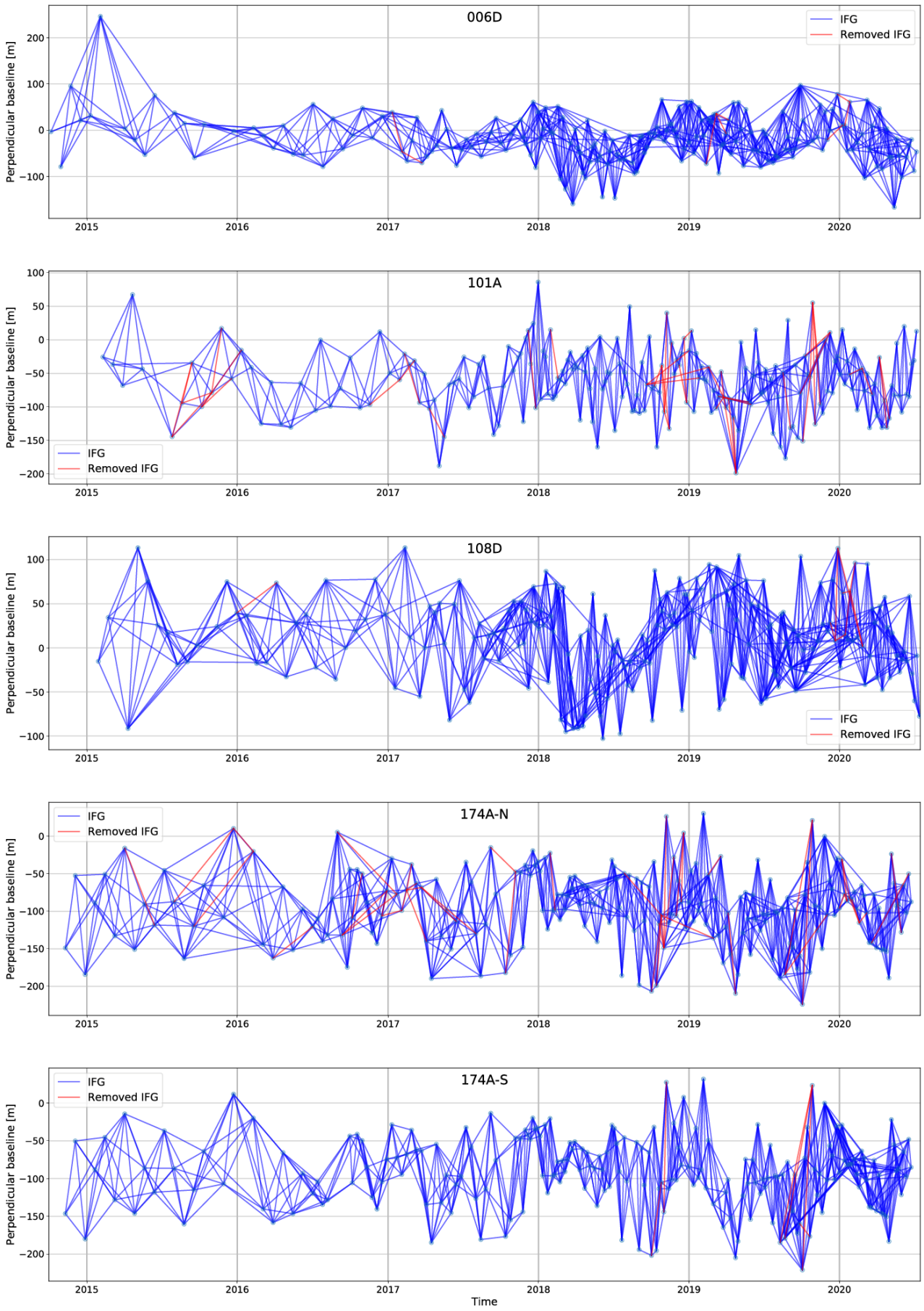

Figure S1: Time series networks for each frame. Blues lines show interferograms between SAR images (blue dots), with red lines showing interferograms that were removed by the LiCSBAS automated quality checks and loop closure. Year labels line up with the beginning of the year.

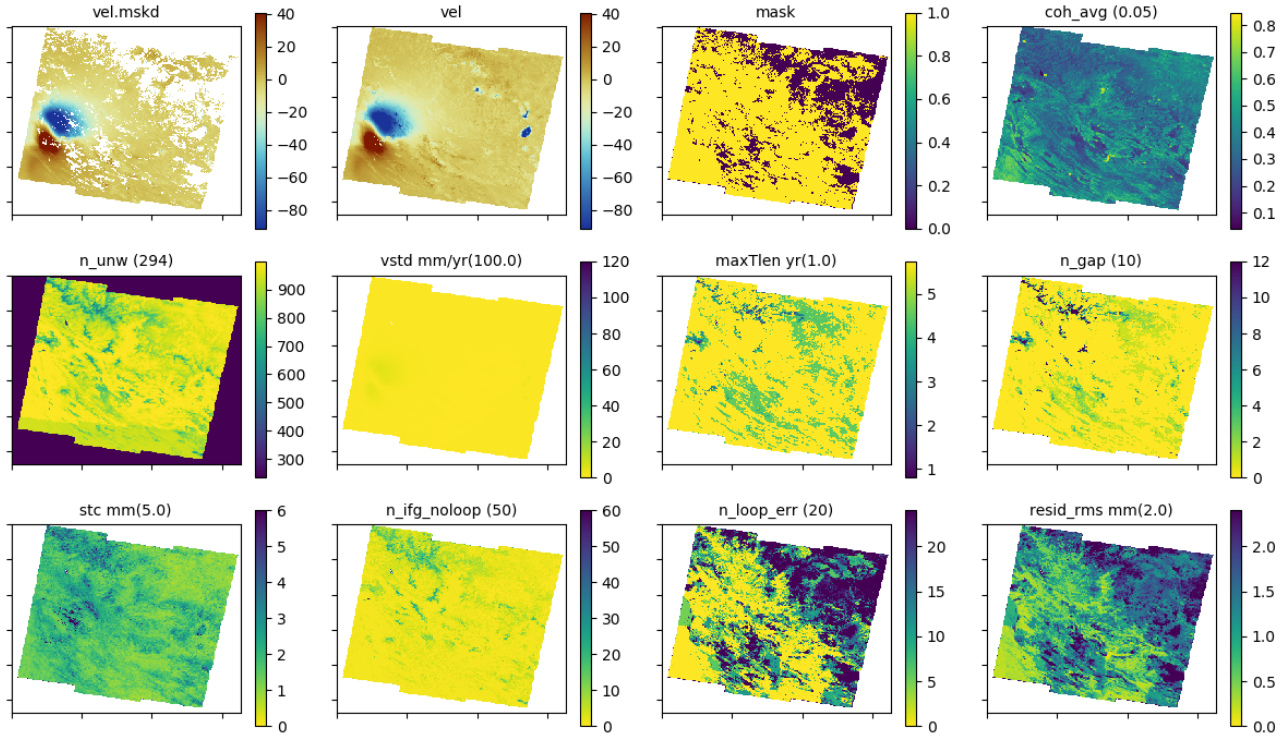

Figure S2: LiCSBAS noise indices for frame 006D_05509_131313, with the threshold for each given in brackets with the title.

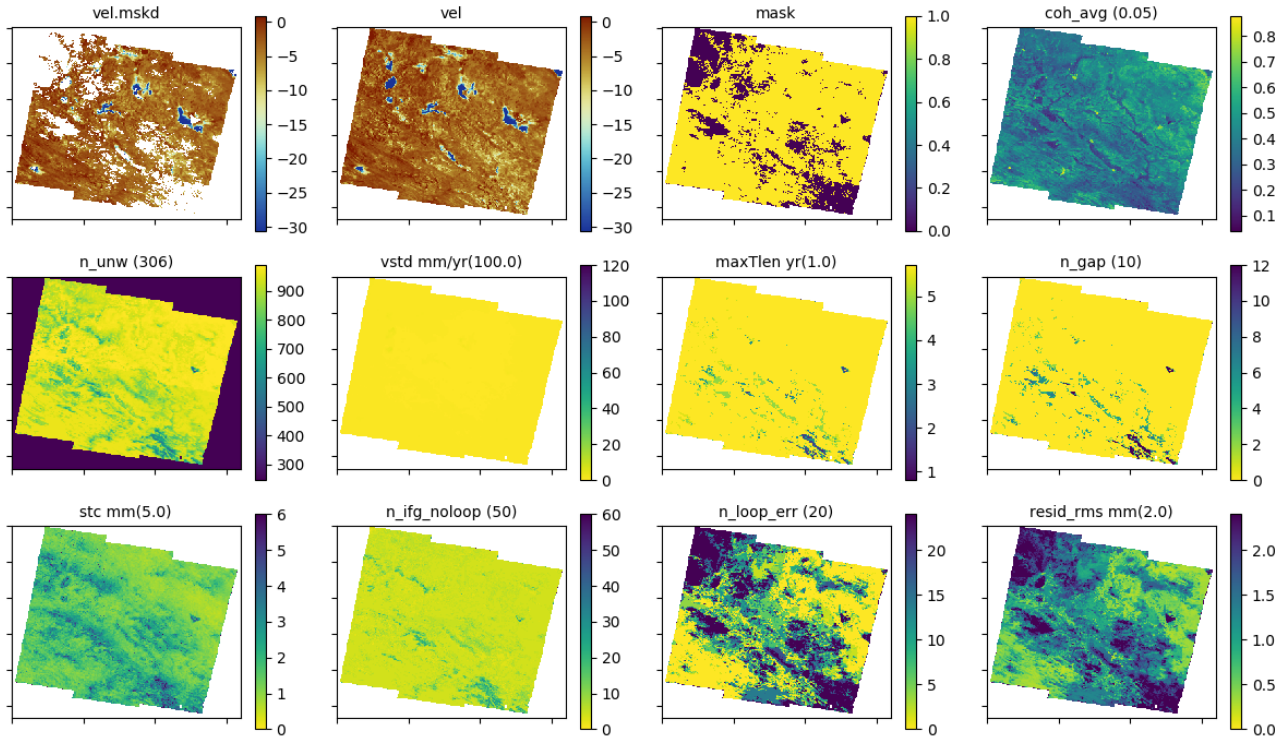

Figure S3: LiCSBAS noise indices for frame 108D_05585_121313, with the threshold for each given in brackets with the title.

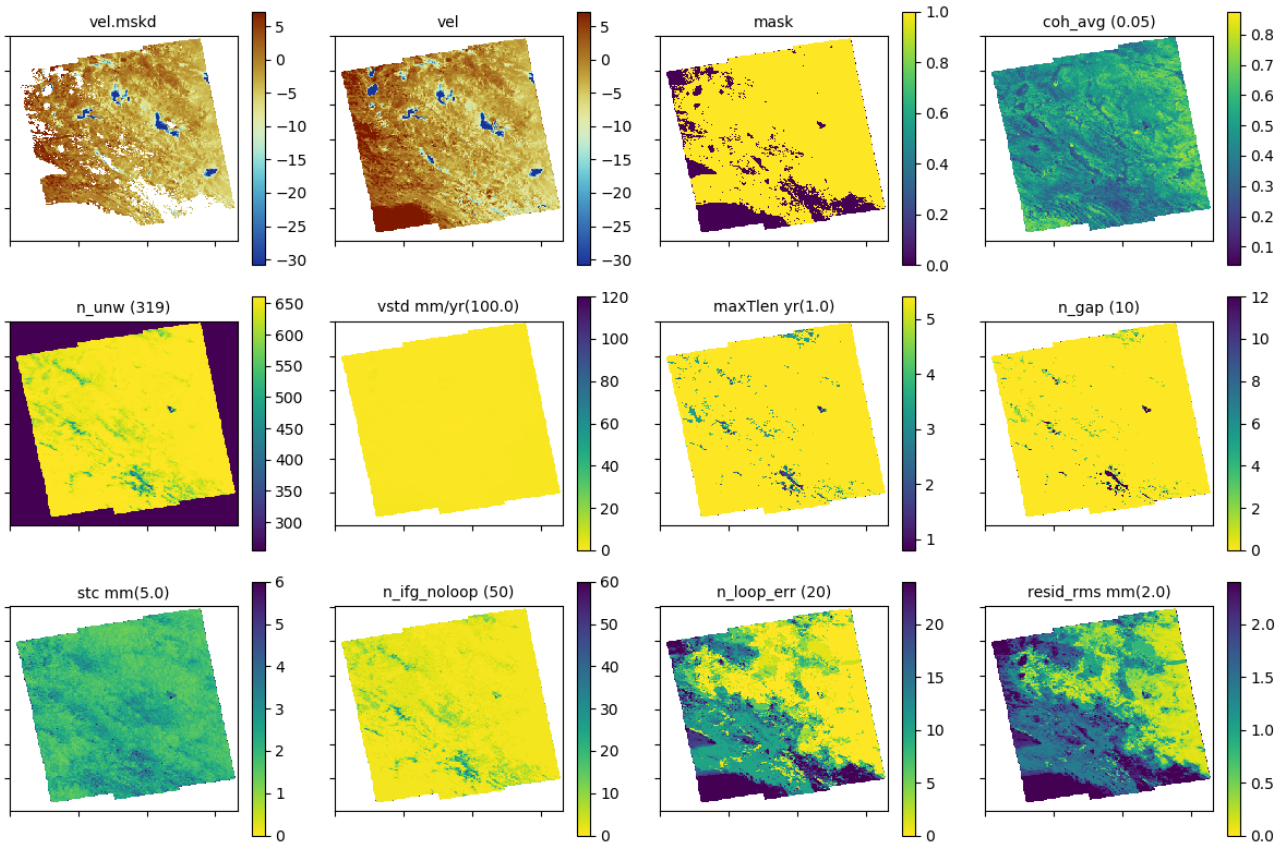

Figure S4: LiCSBAS noise indices for frame 101A_05600_141515, with the threshold for each given in brackets with the title.

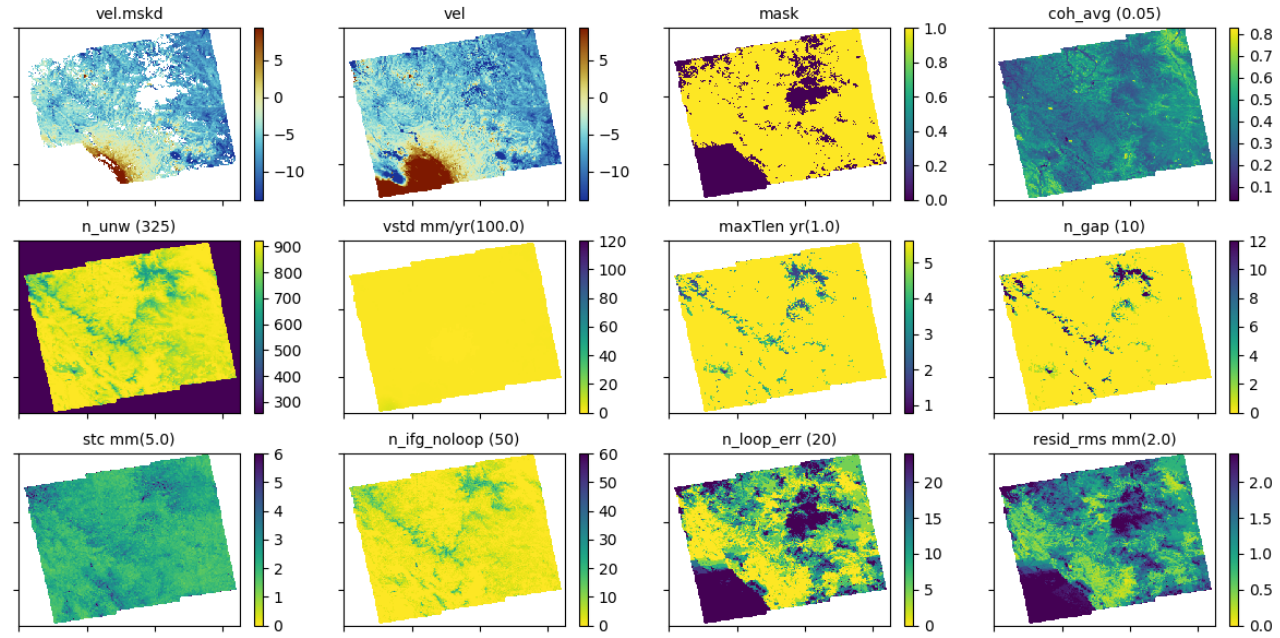

Figure S5: LiCSBAS noise indices for frame 174A_05407_121212, with the threshold for each given in brackets with the title.

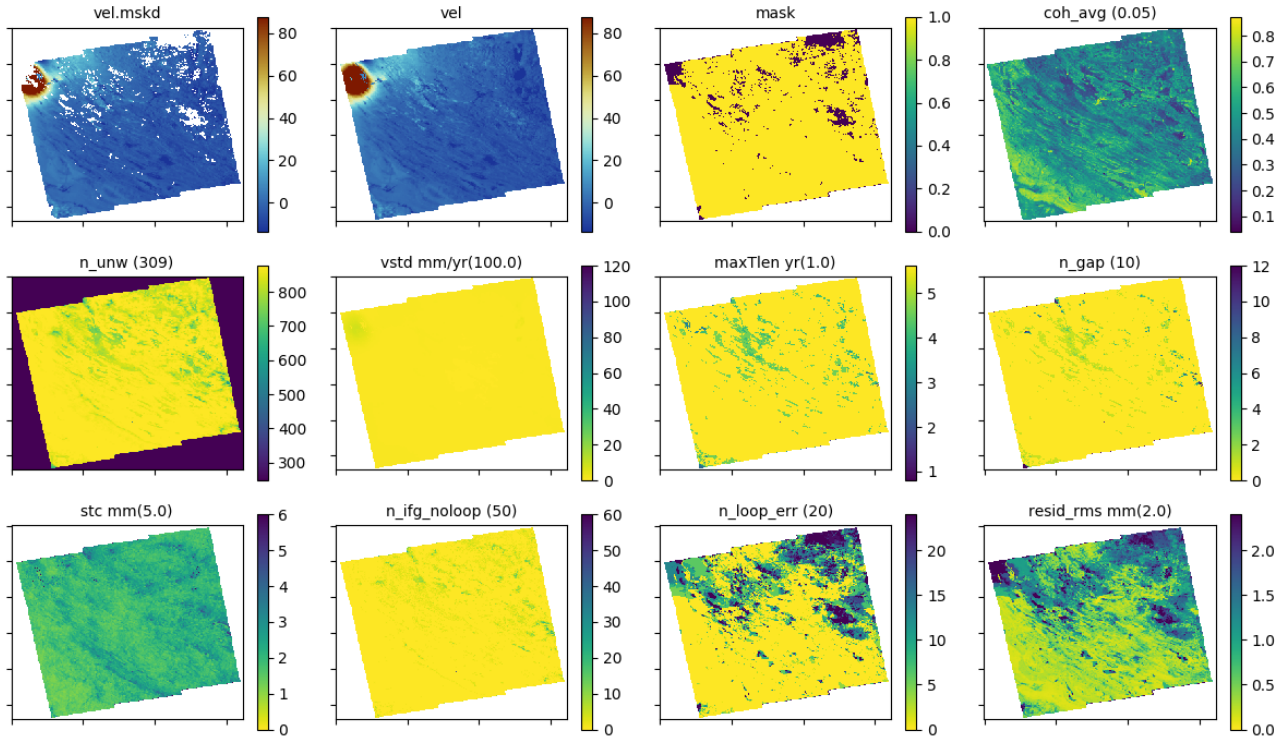

Figure S6: LiCSBAS noise indices for frame 174A_05598_131313, with the threshold for each given in brackets with the title.

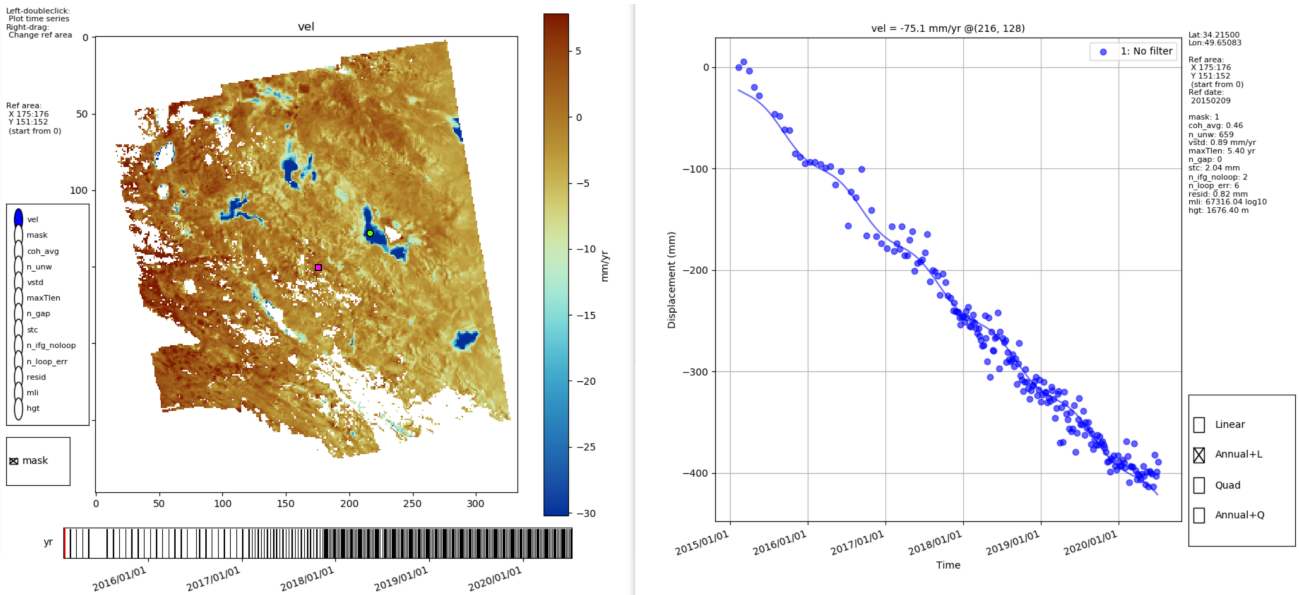

Figure S7: Example LiCSBAS time-series plot for frame 101A_05600_141515. The left panel shows the average line-of-sight velocities relative to the reference pixel (pink square). The right panel shows the cumulative displacement series for a pixel (green circle) within a subsiding basin, with the average velocity given above. The blue line is a linear trend with an annual sinusoidal term.

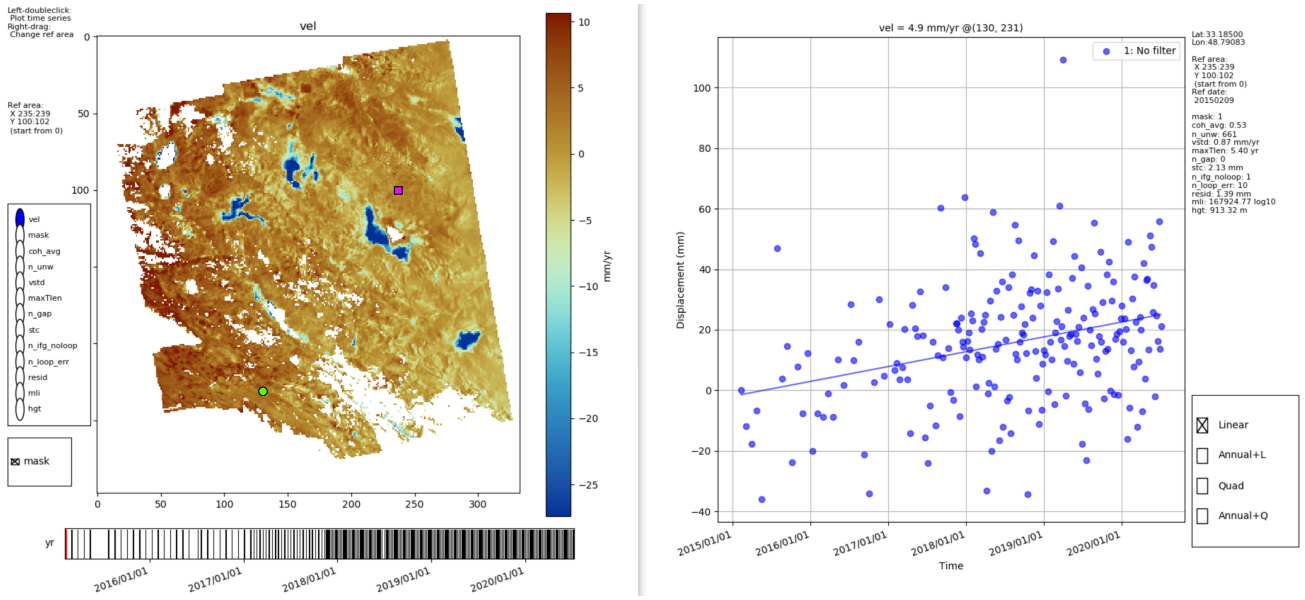

Figure S8: Example LiCSBAS time-series plot for frame 101A_05600_141515. The left panel shows the average line-of-sight velocities relative to a manually selected reference pixel (pink square). The right panel shows the cumulative displacement series for a pixel on the other side of the Main Recent Fault (green circle), with a linear trend and the average velocity given above.

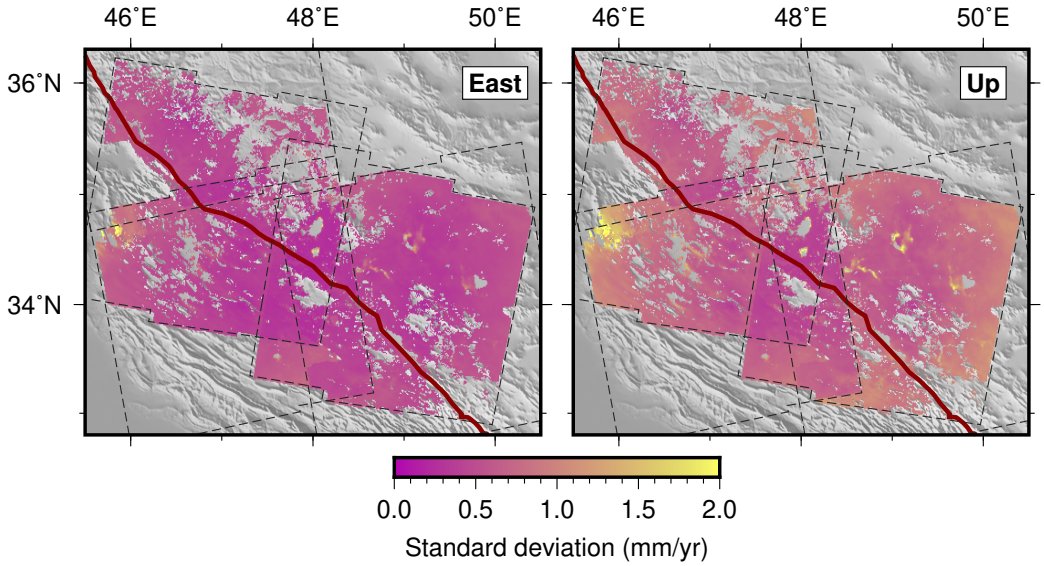

Figure S9: Standard deviation of the decomposed East and Up velocities. Trace of the Main Recent Fault (red line) and the frames outlines (dashed black lines). The uncertainty is generally lower in the centre (around 48° E) where up to four frames overlap, and larger in areas with high average velocity (e.g. the Sarpol-E Zahab earthquake around 46° E, subsidence signals around 49° E) where the disagreement between overlapping frames is the largest.

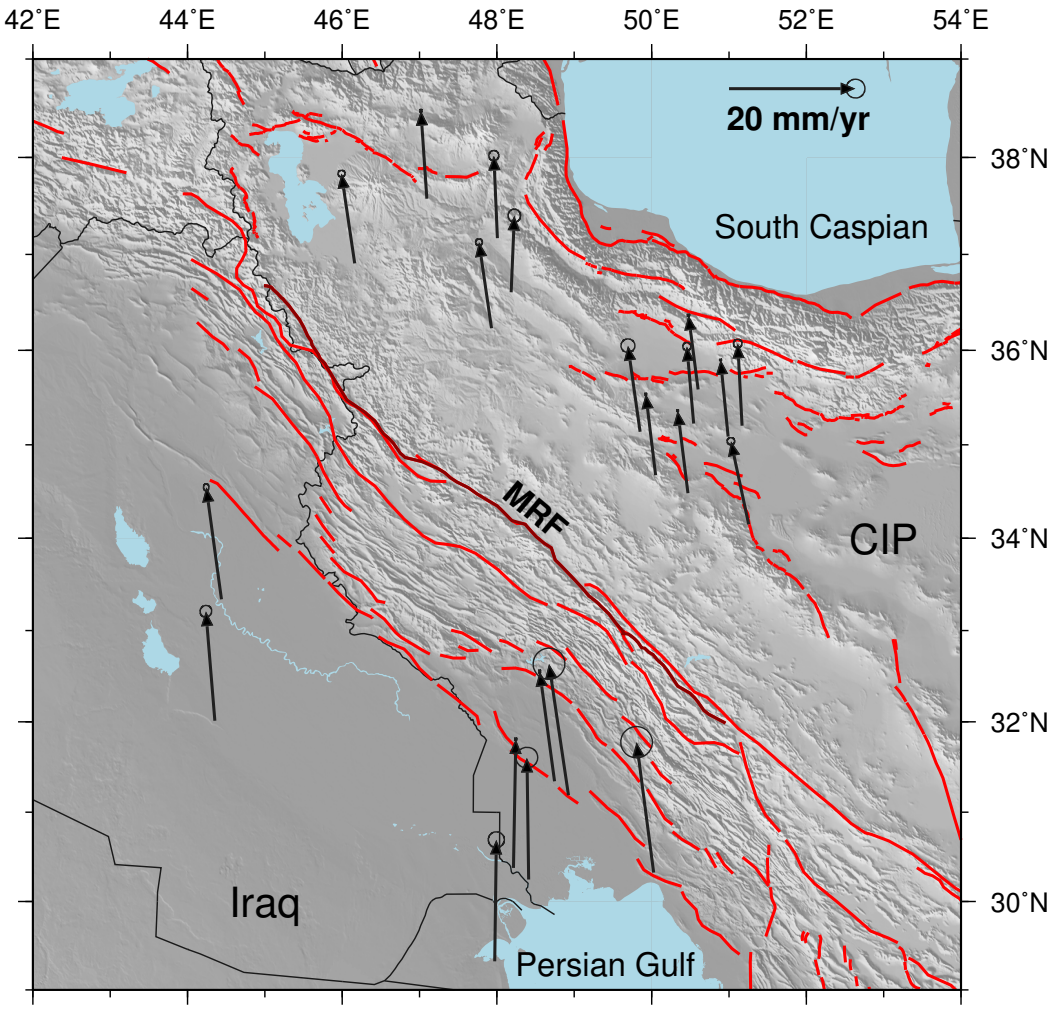

Figure S10: GNSS velocities (relative to stable Eurasia) from Khorrami et al. (2019) used to estimate the velocity difference across the western Zagros, given with 1σ uncertainties. Stations are located at the tail of the arrow. Location of major faults (red lines) from Walker et al. (2010), with the Main Recent Fault (MRF) shown in dark red. CIP = Central Iranian Plateau.

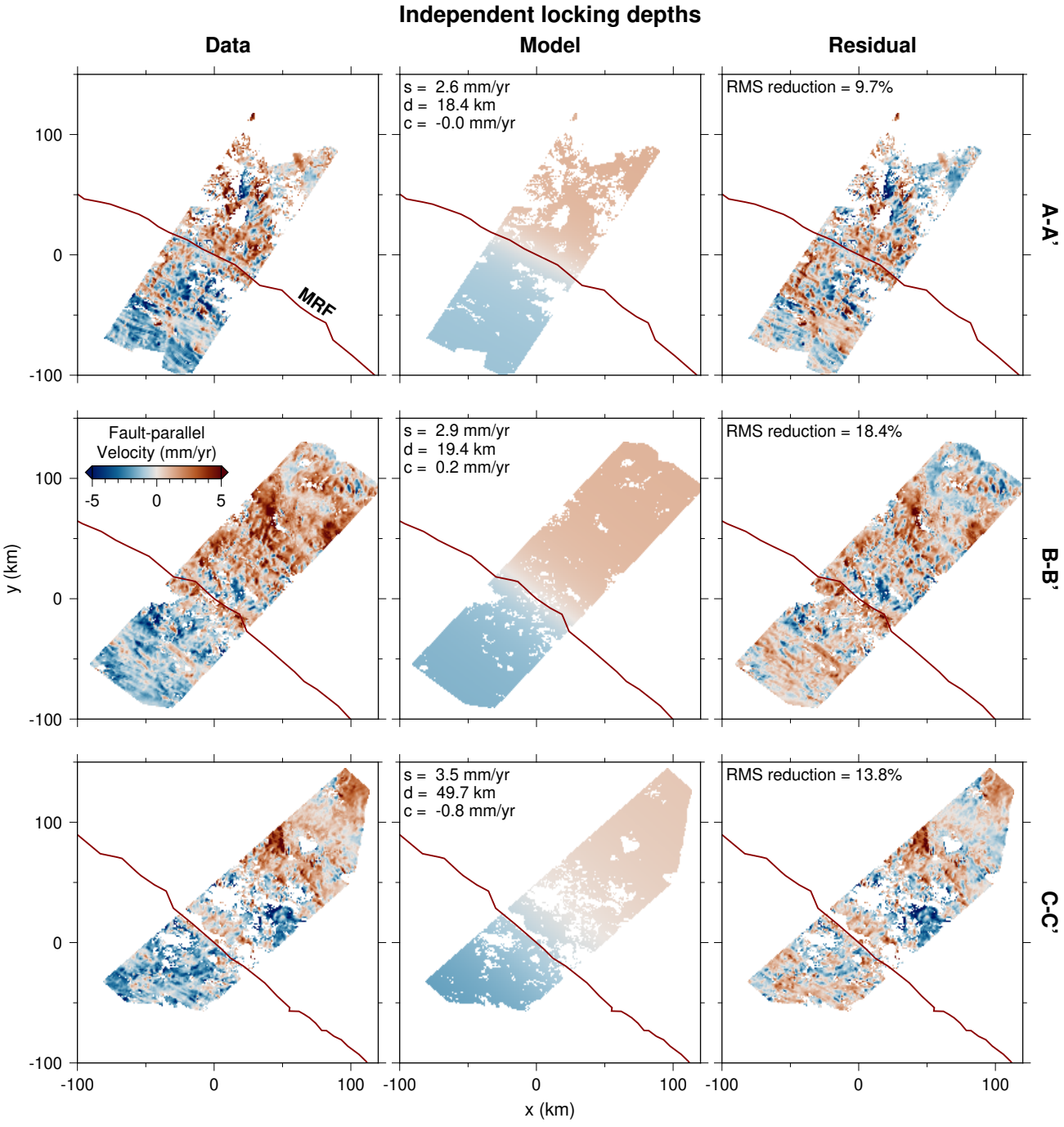

Figure S11: Observed, modelled, and residual fault-parallel velocities for each profile (A-A', B-B', and C-C', see Figure 7) across the MRF (red line). Model velocities are calculated using a screw dislocation (Equation 5) with maximum a posteriori probability (MAP) parameter values for slip (s), locking depth (d), and offset (c), as given in Table 3 and Figure 8, assuming independent locking depths. The reduction in the root-mean-square (RMS) of the velocities is a measure of the fit of the model to the observed velocities. The plot coordinates have been centred on the intersection of the profile line with the fault trace of the MRF.

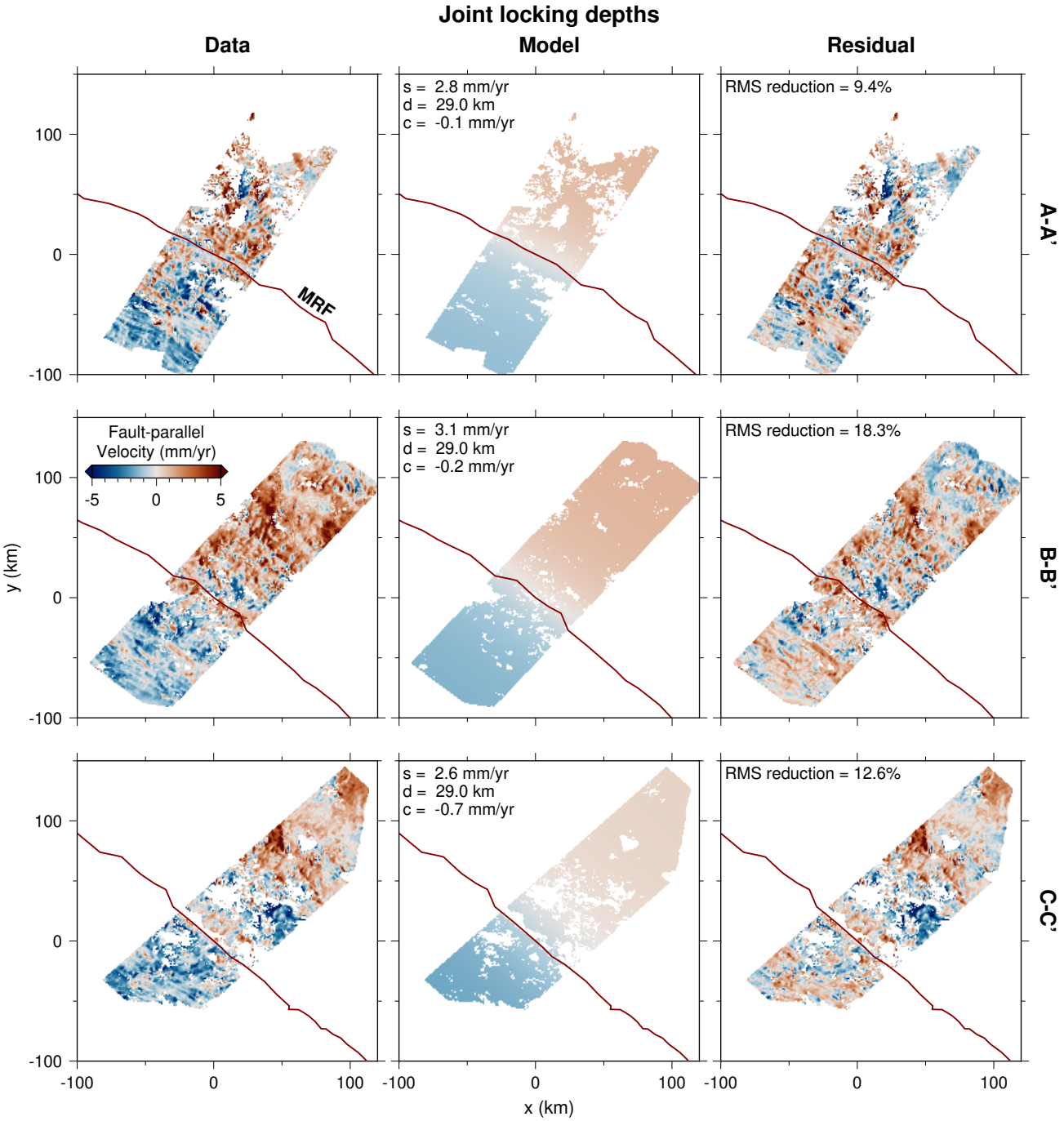

Figure S12: Observed, modelled, and residual fault-parallel velocities for each profile (A-A', B-B', and C-C', see Figure 7) across the MRF (red line). Model velocities are calculated using a screw dislocation (Equation 5) with maximum a posteriori probability (MAP) parameter values for slip (s), locking depth (d), and offset (c), as given in the Table 3 and Figure 10, assuming a single joint locking depth. The reduction in the root-mean-square (RMS) of the velocities is a measure of the fit of the model to the observed velocities. The plot coordinates have been centred on the intersection of the profile line with the fault trace of the MRF.

Table S1: Fault parameters for the 12 November 2017 Sarpol-e Zahab $Mw7.3$ earthquake (Nissen et al., 2019) and associated aftershock sequences on 11 January 2018 and 25 November 2018 (Lv et al., 2020).

Event	Strike	Dip	Rake	Length (km)	Top depth (km)	Bottom depth (km)	Slip (m)
Mainshock	353.7°	14.3°	136.8°	40.1	12.2	17.4	3.05
Aftershocks 1	344°	51°	−78.4°	12.9	13.0	17.2	0.40
Aftershocks 2	302°	90°	−9.2°	12.7	22.0	30.8	1.82